Broadband Chaotic Signals and Breather Oscillations in an Optoelectronic Oscillator Incorporating a Microwave Photonic Filter

Bruno Romeira, *Member, IEEE*, Fanqi Kong, *Student Member, IEEE*, Wangzhe Li, *Student Member, IEEE*, José M. L. Figueiredo, *Member, IEEE*, Julien Javaloyes, *Member, IEEE*, and Jianping Yao, *Fellow, IEEE, Fellow, OSA*

***Abstract*—We propose a technique to generate broadband chaotic and breather signals employing an optoelectronic oscillator (OEO) comprising a phase modulator (PM) and a linearly chirped fiber Bragg grating (LCFBG). The joint operation of the PM and the LCFBG forms a broadband microwave photonic filter (MPF), which allows the OEO to generate chaotic signals and breathers taking advantage of the interplay between the broadband MPF and the time-delayed feedback loop provided by a long optical fiber delay line. The breather excitations are characterized by nanosecond chaotic oscillations breathing periodically at a significantly lower time-scale determined by the OEO large delay time. A theoretical analysis based on a modified Ikeda time-delayed model to include the effect of the broadband filtering process is provided. The analysis is verified by an experiment. The proposed LCFBG-based OEO and the possibility to control in the optical domain its broadband bandpass characteristics considering the flexibility, accuracy, and precision in FBG fabrication can find applications in chaos-based communications and in fast optical processing systems, such as random number generation, or optical processing in reservoir computing taking advantage of the intrinsic multiple time scales of the LCFBG-based OEO.**

***Index Terms*—Fiber bragg grating (FBG), microwave generation, microwave photonics, nonlinear dynamics, optoelectronic oscillator (OEO), phase modulation (PM).**

I. Introduction

COMPLEX oscillatory patterns have been observed in a wide diversity of physical, chemical, biological and engineering time-delay feedback systems [1]. The generation of ultra-wideband optical chaotic signals in microwave-photonics systems using either chaotic semiconductor lasers [2] or optoelectronic oscillators (OEOs) [3] has received considerable interest because it can find a wide-ranging of applications such as in optical chaos secure communications [4], chaotic light detection and ranging (LIDAR) [5], optical time domain reflectometry [6], random bit generation [7], and photonic ultra-wideband signal generation and processing [8].

A number of photonic microwave generation techniques have been extensively investigated showing that adding a delayed feedback loop to a system can stabilize the output producing highly stable periodic waveforms [9], [10], or exceedingly complex dynamics [11], depending on the gain and delay parameters. The effect of the delayed feedback is to reinject into the system one or more state variables with a delay providing diverse oscillating outputs [12]. Within the field of laser dynamics, the most prominent examples are the optoelectronic feedback and the optical feedback [13]. Although chaotic semiconductor laser systems have been successfully demonstrated in chaos synchronization for secure optical communications, the required synchronization is very sensitive to laser physical parameters [4], which makes its implementation still very challenging.

Alternatively, an OEO can generate photonic microwave signals with excellent frequency stability through attaining a high quality factor using a very long fiber loop [14], and also produce broadband chaotic signals [3]. Nowadays, the number of reported OEO architectures is considerably large and spans from OEOs based on modulators [3], to implementations using whispering gallery mode cavities [15], and utilizing self-injection locking of microwave oscillators for compact OEOs [16], to cite only a few (for a recent review see [17]). Among the various implementations, the electro-optical feedback loop composed by a Mach–Zehnder modulator (MZM), a continuous-wave (CW) semiconductor laser, an optical fiber delay line, a photodiode (PD), and an electrical amplifier (EA) is one of the most widely studied architectures not only for chaos generation [3], but also for the generation of complex temporal patterns such as chaotic breathers [18], and excitable self-pulsating signals [19], to name only a few. Their use for chaos generators have been proven to provide robust operation in both electrical and optical domains and better performance in terms of bit rate capabilities [4]. However, in applications such as chaos encryption, intensity modulation has a critical issue due to undesired interference phenomena [4], so phase-modulation-based OEOs have been also proposed [20]. Recently, extensive work has been reported

Manuscript received January 15, 2014; revised February 20, 2014; accepted February 22, 2014. Date of publication February 24, 2014; date of current version September 1, 2014. This work was supported in part the National Science and Engineering Council of Canada. The work of B. R. was supported by a Postdoctoral Fellowship from FCT Portugal under Grant SFRH/BPD/84466/2012. The work of J. J. was supported by the Ramón y Cajal Fellowship.

B. Romeira is with the Microwave Photonics Research Laboratory, School of Electrical Engineering and Computer Science, University of Ottawa, Ottawa, ON K1 N 6N5, Canada and the Center of Electronics, Optoelectronics and Telecommunications, Department of Physics, University of the Algarve, 8005-139 Faro, Portugal (e-mail: bmromeira@ualg.pt).

F. Kong, W. Li, and J. Yao are with the Microwave Photonics Research Laboratory, School of Electrical Engineering and Computer Science, University of Ottawa, Ottawa, ON K1 N 6N5, Canada (e-mail: jpyao@eecs.uottawa.ca).

J. M. L. Figueiredo is with the Center for Electronics, Optoelectronics and Telecommunications, Department of Physics, University of the Algarve, 8005–139 Faro, Portugal.

J. Javaloyes is with the Departament de Fisica, Universitat de les Illes Baleares, Palma E-07122, Spain.

Color versions of one or more of the figures in this paper are available online at http://ieeexplore.ieee.org.

Digital Object Identifier 10.1109/JLT.2014.2308261

0733-8724 © 2014 IEEE. Personal use is permitted, but republication/redistribution requires IEEE permission.
See http://www.ieee.org/publications_standards/publications/rights/index.html for more information.

on novel OEO architectures combining a phase modulator (PM) and a linearly chirped fiber Bragg grating (LCFBG), forming a microwave photonic filter (MPF) for the generation of high-purity microwave signals [21], [22], but the possibility of chaos generation and other complex signals as the ones reported here, taking advantage of the broadband bandpass characteristics of an LCFBG-based OEO, to the best of our knowledge, has not been investigated.

In this paper, we propose and demonstrate an OEO with an ultra-wide bandwidth implemented using a PM and a LCFBG for the generation of broadband chaotic and breather signals based on electro-optic phase modulation. The joint operation of the PM and the LCFBG allows to obtain phase-modulation to intensity-modulation (PM–IM) conversion, leading to a MPF with an ultra-wide bandwidth. Although a PM-based OEO has been proposed for chaotic signal generation [20], the key difference between the proposed approach here and the previously reported PM-based approach [20], is that the use of a PM and a LCFBG provides the possibility to control in the optical domain the characteristics of the broadband MPF which can be employed to tailor the broadband chaotic dynamical regimes without requiring further changes of the characteristics of the other components of the OEO.

A theoretical analysis based on a modified Ikeda time-delayed model to include the effect of the broadband filtering process is performed. The model consists of an integro-differential time-delay equation describing a supplementary slow time scale arising from the MPF effect when compared with the original proposed Ikeda dynamical model [23]. Numerical simulations show that by taking advantage of the interplay between the broadband MPF and the time-delayed feedback loop provided by a large optical fiber delay line, the generation of chaotic signals and breather signals can be achieved. The analysis is verified by an experiment. The breather excitations reported here are characterized by nanosecond chaotic oscillations breathing periodically at a significantly lower time-scale controlled by the OEO large delay time, and are a special hybrid-type dynamics which has a characteristic similar, for example, to the biological neuronal fast-slow bursting phenomena [24], [25]. This makes the breathing phenomena to be the object of a remarkable multidisciplinary interest with respect to fields as diverse as biophysics (e.g., nerve fibers [26] and neuronal response [25]), nonlinear optics (photonic crystals and waveguides [27], [28]), and electro-optic oscillators [18], [19].

II. Operation Principle

The proposed time-delayed OEO for ultra-wideband optical chaotic signal generation is schematically shown in Fig. 1. It consists of a tunable laser source (TLS) (1440–1640 nm) providing up to 8 dBm optical power output, a polarization controller, a broadband PM with a modulation bandwidth of 20 GHz and a half-wave voltage $V_{\pi \mathrm{RF}} = 4.5$ V, an LCFBG, an optical circulator (OC), an optical fiber delay line, an erbium-doped fiber amplifier (EDFA), a variable optical attenuator (VOA), a PD (10 GHz) with a responsivity of 0.82 A/W at 1550 nm, and an EA. The LCFBG has a 3-dB bandwidth of 0.56 nm, a dispersion

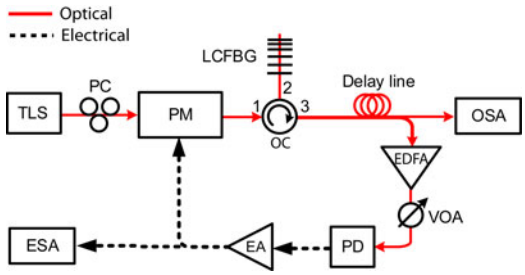

Fig. 1. Schematic of the OEO employing a PM and a LCFBG in a time-delayed feedback loop.

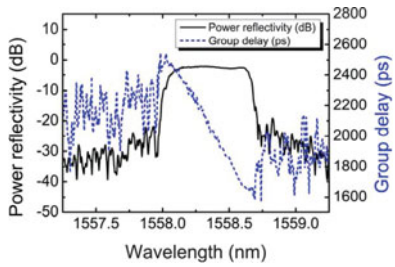

Fig. 2. Power reflectivity and group delay spectra of the LCFBG exhibiting a 3-dB bandwidth of 0.56 nm and dispersion around 1457 ps/nm.

value of 1457 ps/nm, and a peak power reflectivity of 95%, as shown in Fig. 2. The EA has an electrical gain of 45 dB and a bandwidth of 30 kHz–10 GHz. A CW light from the TLS is sent to the broadband PM. The PM represents one of the key elements of the OEO acting as a fast electrical-to-optical converter. The phase-modulated light at the output of the PM is then sent to the LCFBG through the OC and then delayed using a single mode fiber of a length of several meters. After amplification by the EDFA, the optical signal is converted to an electrical signal at the PD. The VOA is employed to tune the optical attenuation and therefore adjusting the gain of the feedback loop. The electrical signal is then linearly amplified by the EA, and then fed back to the PM to close the OEO loop. The signal generated by the OEO is monitored in the electrical domain using an electrical spectrum analyzer and a fast real-time digital oscilloscope, and in the optical domain by an optical spectrum analyzer (OSA). For clarity, the description of the components employed in the OEO and other acronyms are listed in Table I.

Depending on the wavelength of the TLS, the OEO can be configured to operate in two regimes. If the wavelength is located in the center of the reflection window of the LCFBG, the phase relationship between the two first-order sidebands of the phase-modulated signal is changed from out of phase to partially or fully in phase due to the dispersion-induce phase change, thus the phase-modulated signal is converted to an intensity-modulated signal. The frequency response of the chromatic-dispersion-based PM-IM conversion is a quasi-periodic function, as shown as the dashed line in Fig. 3. The frequency response between the first two notches forms a passband MPF. The profile of the open-loop response is mainly determined by the dispersion-induced MPF which has a 3-dB bandwidth of about 3.5 GHz. Highly-stable single tone oscillations have been demonstrated employing this regime of operation [21], [22].

TABLE I
ABBREVIATIONS AND ACRONYMS LIST

Acronym	Definition
CW	Continuous wave
DDE	Delay differential equation
EA	Electrical amplifier
EDFA	Erbium-doped fiber amplifier
ESA	Electrical spectrum analyzer
LCFBG	Linearly chirped fiber Bragg grating
LIDAR	Light detection and ranging
MPF	Microwave photonic filter
MZM	Mach-Zehnder modulator
OC	Optical circulator
OEO	Optoelectronic oscillator
OSA	Optical spectrum analyzer
PC	Polarization controller
PD	Photodiode
PM	Phase modulator
PM-IM	Phase-modulation to intensity-modulation
RF	Radio-frequency
TLS	Tunable laser source
VOA	Variable optical attenuator

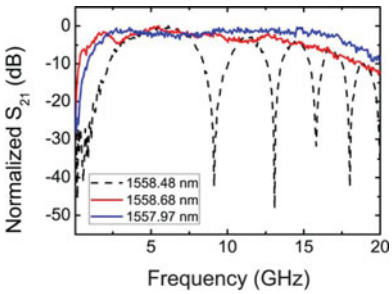

Fig. 3. Spectral response of the OEO open loop.

On the other hand, when the wavelength of the light wave is placed at one of the positive or negative slopes of the LCFBG optical filter, as shown in Fig. 2, it leads to the elimination of one of the two sidebands, as shown in Fig. 4(a). As a result, the phase-modulated signal is converted to a single-sideband intensity-modulated signal, as presented in Fig. 4(b) and (c). It has been demonstrated in previous work that in this regime of operation the LCFBG can be used as a frequency discriminator [29]. The frequency responses of the LCFBG when the wavelength is located on the right downward slope ($\lambda = 1558.68$ nm), and in the left upward slope ($\lambda = 1557.97$ nm) are shown in Fig. 3. As can be seen the frequency response in this case exhibits a flat gain with only one passband instead of multiple resonance peaks, which differs substantially from the spectral response when the wavelength is located in the flat region of the reflection window. When located within the LCFBG window, the two sidebands as a function of the frequency will sometimes be in phase, then anti-phase, then in phase again due to the group velocity dispersion of the LCFBG, which gives the various resonance peaks displayed in Fig. 3. However, when the wavelength is located in one of the LCFBG slope regions, a destructive interference will never occur since the opposite sideband was suppressed.

Therefore, if the wavelength of the optical carrier is properly selected to make it located at one of the slopes, a wideband OEO is realized, with a bandwidth that can go above 1 nm by taking advantage of the large reflection window of the LCFBG.

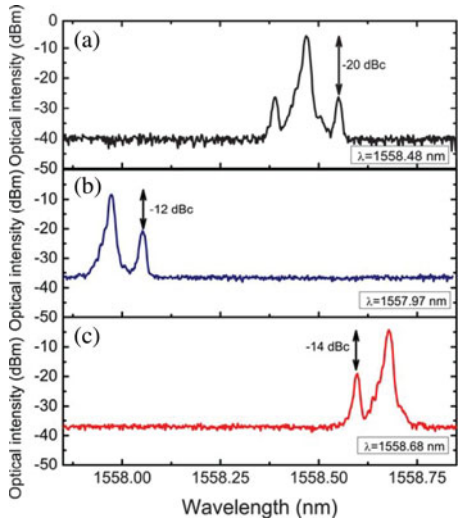

Fig. 4. Measurements of the spectral response of the OEO open loop when the PM is driven by a 10-GHz electrical signal. (a) Dual sideband modulation when the wavelength is located in the reflection window of the LCFBG; (b) single-sideband modulation when the optical wavelength is located at the left and (c) right slope of the LCFBG.

The equivalent frequency bandwidth, corresponding to more than 100 GHz, is much higher than the bandwidth of the electronic components usually employed in the OEO, which makes this regime of operation particularly suitable for the generation of ultra-wideband phase-chaotic signals, and other complex microwave-photonics signals such as breather excitations that arise from the interplay between the multiple fast and slow scale dynamics.

III. NUMERICAL MODEL

Developing a computational model of the broadband OEO described here capable of reproducing and predict the diverse complex oscillatory dynamics observed experimentally is a challenging task because of the large separation between the slow and fast time-scales in the electro-optic system. There are three different time-scales in our OEO: the microwave carrier frequency in the GHz range, the filter low cutoff frequency in the MHz range, and the free spectral range in the kHz range. Because the time delay (typically in the μs range) is much higher than the time scale of the oscillation frequency of the OEO, long run simulations and large amount of memory storage are usually required in the analysis of these type of delayed systems leading to long time consuming simulations. Furthermore, chaos and other complex non-periodic regimes are only frequently observed when the OEO operates under moderate or strong feedback gain conditions, which makes analytical analysis very demanding.

In this Section, we model our OEO using a modified Ikeda time-delayed equation which describes the three different scales of the OEO. The Ikeda-type nonlinearity with delayed feedback was originally proposed to model a passive optical bistable resonator system [23] and is given by

$$\tau \frac{dx}{dt}(t) + x(t) = \beta \sin\left[x(t-\tau_d) - x_0\right] \tag{1}$$

where $x(t)$ represents a scalar variable of the system under analysis. The left-hand side describes a linear filtering process with a characteristic time τ, and the right hand-side represents a nonlinear delayed feedback term with a time delay τ_d, weighted by the gain feedback parameter β; x_0 describes a constant phase offset.

The Ikeda nonlinearity is often encountered in electro-optical systems. However, recent work [18], [19], [30] demonstrates that a number of complex dynamics is absent in the classical first-order nonlinear delay differential equation (DDE) presented in (1) characterized solely by a high cutoff frequency. In order to capture the dynamics observed experimentally, specifically the fact that in our OEO the MPF and the frequency response of the electronic and optoelectronic components induce a bandpass property, we assume that the frequency filtering process can be modeled in the time domain by an integro-differential operator characterized by both high- and low-cut off frequencies. In our analysis, we consider our OEO as an experimental realization of a modified Ikeda time-delayed equation and it is modeled employing a bandpass nonlinear dynamical system [19], [30]. To simplify the analysis, we assume that the filter is linear and of second order (see also [19], [31] where similar bandpass dynamical models are employed). Specifically, in our OEO system the dynamical behavior can be described by an integro-differential equation so that the dynamics of the radio-frequency (RF) voltage $V(t)$ at the input of the PM [31] reads as

$$\tau\frac{dV}{dt}(t)+V(t)+\frac{1}{\theta}\int_{t_0}^{t}V(t')dt' = \gamma K^2 G_0 \Re P_0 \sin\left[\frac{\pi V(t-\delta\tau_0-\tau_d)}{V_{\pi\mathrm{RF}}}+\frac{2\pi\delta\tau_0}{\lambda_0}\right]. \quad (2)$$

The left-hand side describes a bandpass filtering process where $\tau = 1/2\pi f_h$ and $\theta = 1/2\pi f_l$ are the characteristic response times associated with the high, f_h, and the low, f_l, cut-off frequencies, respectively. Note that the condition of $\tau \ll \theta$ has been taken into account in (2) which is an easily fulfilled assumption considering the wideband filtering provided by the MPF and the broadband characteristics of the remaining OEO components. The right hand-side represents the Ikeda-like nonlinearity delayed feedback term with a time delay τ_d that originates from the optical fiber delay line and partly from the electronics, weighted by the gain feedback which depends on the following parameters of the OEO: γ accounts for the optical power losses; K is the slope steepness factor of the LCFBG; $\Re$ is the responsivity of the PD, P_0 is the optical intensity input, and G_0 stands for the amplifier gain. At last, in (2), $\delta\tau_0$ is the group delay where typically $\delta\tau_0 \ll \tau_d$ for a significantly large delay time, $\beta_{\mathrm{PM}} = \pi/V_{\pi\mathrm{RF}}$ is the phase modulation index, where $V_{\pi\mathrm{RF}}$ is the half-wave voltage of the PM, and $\phi_0 = 2\pi\delta\tau_0/\lambda_0$ is a constant offset phase, where λ_0 stands for the wavelength of the optical carrier.

For mathematical convenience we introduce a dimensionless variable as follows

$$x(t) = \pi\frac{V(t)}{V_{\pi\mathrm{RF}}}. \quad (3)$$

TABLE II
DEFINITIONS OF THE PHYSICAL AND MODELING PARAMETERS OF THE LCFBG-BASED OEO

Parameter	Value	Meaning
τ_d	300 ns	Delay
τ	15 ps	High frequency cutoff
θ	5 ns	Low frequency cutoff
P_0	0 – 6.3 mW	Optical intensity input
$\Re$	0.82 A/W	Responsivity of PD
γ	0.09	Optical losses parameter
β	0 – 4.0	Normalized feedback gain
$V_{\pi RF}$	4.5 V	Half-wave RF voltage
ϕ_0	π/4 rad	Offset phase
λ_0	1558.68 nm	Wavelength of the optical signal

The dimensionless dependent variable $x(t)$ is proportional to the signal in the electronic feedback driving the PM. Considering a dimensionless time scale t/τ normalized to the delay we can write (2) in a more convenient 2-D vectorial form with dimensionless parameters

$$\begin{aligned} x' &= -\varepsilon y - x + \beta\sin\left[x(t-T)+\chi\xi(t)+\phi_0\right] \\ y' &= x \end{aligned} \quad (4)$$

where $\varepsilon = \tau/\theta$ is the ratio between the low and high cut-off frequencies, ϕ_0 is a constant offset phase, $\beta = \pi\gamma K^2 G_0 \Re P_0 / V_{\pi\mathrm{RF}}$ is the overall feedback gain, and T the total delay time. For clarity, the meaning and values of the physical and modeling parameters are listed in Table II.

The resulting (4) can be described as a modified Ikeda-like DDE that includes the effect of the MPF bandpass filtering process. Furthermore, in real OEO systems the unavoidable noise sources can affect the system dynamics by introducing amplitude and phase fluctuations even in the most stable periodic signals. In our case, several sources or random processes are at play, such as thermal and shot noises. We model their overall effect as an effective delta-correlated Gaussian white noise of zero mean $\chi\xi(t)$ [32], where the parameter χ is the dimensionless variance of the distribution and denotes the noise strength.

For purposes of numerical simulation, the DDE system represented by (4) is integrated with a standard constant step size Runge–Kutta method of fourth order [33]. As discussed previously, since long run simulations and large amount of memory storage are required to solve DDE, we interface a C++ time integrator with MATLAB & Octave [34] via the mex interface [27]. This allows for high performances, efficient scripting capabilities as well as easy cluster deployment, three characteristics that are useful for extended parametric studies. The presence of a delayed contribution in (4) demands a special care. Indeed, to advance the solution with a time step h from $t_n = nh$ to $t_{n+1} = (n+1)\,h$, the Runge–Kutta algorithm requires evaluating the values of $x = (t-T)$ at intermediate points $t_{\mathrm{mid}} = (n+1/2)\,h$. However, $x = (t_{\mathrm{mid}} - T)$ is not known and must be interpolated from past values, e.g., $x = (t_{n-1} - T)\,, x = (t_n - T)\,, x = (t_{n+1} - T)$, with an

order consistent with the algorithm of integration. Therefore, in addition to the past values of $x(t)$ we also kept the time derivative $\dot{x}(t)$, that is, a quantity readily available upon time integration which allows building a third order Hermite polynomial between $t_n - T$ and $t_{n+1} - T$. By evaluating this interpolation of the delayed term at $t_{\mathrm{mid}} - T$, we ensure an overall fourth order accuracy. The stochastic component contribution $\chi\xi(t)$ in (4) is added after the deterministic step by using the Euler method [32].

In what follows, we will discuss numerically and experimentally how the interplay between the three time scales of the OEO-based MPF gives rise to a large variety of oscillatory regimes and complex dynamical behaviors.

IV. Results

An experiment is performed based on the setup shown in Fig. 1. We start by selecting the wavelength of the light source ($\lambda = 1558.68$ nm) at the right slope of the LCFBG reflection window. The output power of the TLS is set at 8 dBm and the maximum power received by the PD is around 0 dBm. The feedback delay is estimated to be $\sim$300 ns and originates mainly from the optical fiber delay line, and the fiber-optic and optical devices, and partly from the electronics. In what follows we investigate the generation of complex microwave-photonics signals which include broadband chaos and breather excitations by varying the feedback gain and time delay conditions of the system.

A. Route to Chaos Dynamics

The route to chaos dynamical scenario beginning with a stable steady state and evolving to the fully developed chaotic regime is analyzed while changing the gain conditions of the OEO. Fig. 5 shows the measured temporal waveforms for long time traces (a few time delays, left figures), and shorter ones (tens of ns), displaying different dynamical states depending on the feedback gain. When the optical power level is very low, the OEO is nearly an open loop and a stable steady state with zero amplitude oscillations is observed, as shown in Fig. 5(a) and (b). For optical power levels received by the PD above –8.6 dBm, the OEO starts to oscillate with an oscillation around 2.8 GHz. The typical two-level oscillation is shown in Fig. 5(c) and its zoom-in view is shown in Fig. 5(d). The observed oscillation frequency appears through an Andronov–Hopf bifurcation, and is the result of the combined MPF together with the amplitude response of the optoelectronic feedback. Analyzing the open loop RF filtering response, a maximum at around 2.8 GHz is observed, thus explaining the actual closed-loop oscillation. The amplitude of the oscillations grows continuously as the optical power is increased, as can be seen from Fig. 5(e) and (f).

When the optical power is further increased in the range of -5.7 dBm to 0 dBm, more complex oscillations, including chaos, are observed. Fig. 5(g) shows an example of the evolution of the dynamics when the optical power is set at -5.6 dBm. Its zoom-in view is shown in Fig. 5(h). In this case, the dynamics is characterized by two successively appearing frequencies with different time scales, one appearing at the fast 2.8 GHz oscillation and the other as a slow envelope modulation related to the total delay of the loop. This transition from periodic to complex regimes resembles the route to chaos of many Ikeda-like dynamics [23]. However, contrary to the typically standard Ikeda dynamics exhibiting period-doubling oscillations, the four-level oscillations observed appear as a result of an additional frequency through a Neimark–Sacker bifurcation [31] where we clearly have a secondary Hopf bifurcation with a frequency that is not half of the fundamental as it would be for the period doubling scenario. This is characteristic of a route to chaos via quasi periodicity and of the so called Ruelle–Takens mechanism. In our case the second low frequency is a consequence of the delay influence being greater. For low feedback, the time-delayed signal sustain a periodic regime of an otherwise damped oscillator, but for large time-delayed feedback, the feedback triggers oscillations at the delay frequency.

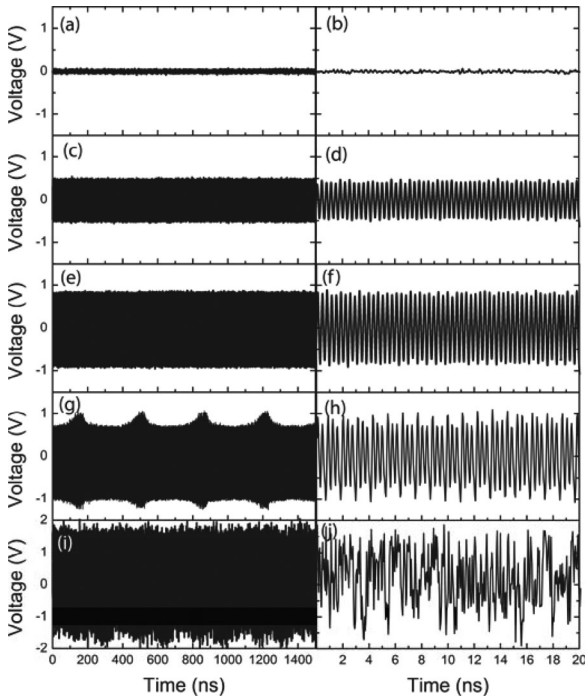

Fig. 5. Experimental time traces of OEO route to chaos dynamics for increasing values of optical power launched in the PD: (a,b) -9.0 dBm; (c,d) -8.4 dBm; (e,f) -6.8 dBm; (g,h) -5.6 dBm; (i,j) -0.5 dBm.

Further increasing the optical power level, and therefore higher feedback gain, the OEO starts to generate broadband signals, a characteristic of deterministic chaotic regimes. Fig. 5(i) and (j) show large amplitude chaotic oscillations [notice the different y-axis scale when compared with Fig. 5(a)–(h)]. The large amplitude waveform is a signature of a strong nonlinear regime. In the chaotic regime observed here, the dynamics typically feature with a broadband spectrum with an all-time scale chaotic time trace (almost noise like), continuously spanning a very broad temporal scale from the slow to the fast characteristic times. Fig. 6 shows a typical RF spectrum covering the full bandwidth of the EA with a substantial rise of the power spectra noise level (up to 40 dB around 2 GHz). The bandwidth of the electronic loop is the major limitation of the achieved

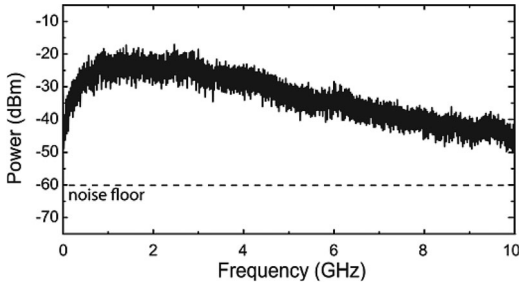

Fig. 6. Experimental power spectrum of the OEO operating in a deterministic chaotic state when the optical power launched in the PD is around −0.5 dBm.

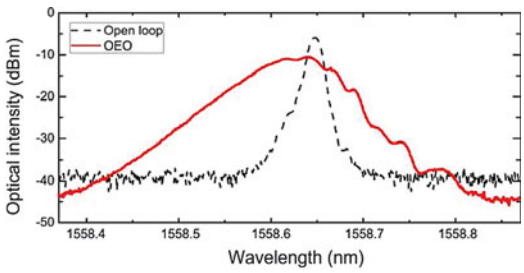

Fig. 7. Experimental optical spectrum of the OEO optical output operating in a deterministic chaotic state when the optical power launched in the PD is around −0.5 dBm. Also shown is the laser free-running frequency when the OEO is operating in open loop.

bandwidth of the chaotic signals generated. In this regime, the optical spectrum is significantly broadened when compared with the free-running laser operating in the open loop as displayed in Fig. 7. These spectral features are characteristic of high complexity chaotic dynamics that are very attractive for high-speed chaos-based communications.

The OEO dynamics observed experimentally employing moderate and high gain conditions is further investigated using numerical simulations of the DDE system given in (4). The DDE system is integrated with a time step of $h = 0.1$, which corresponds to a $dt = 1.5$ ps, over N round trips in the optoelectronic feedback loop. At each round trip the signal is propagated in the OEO and computed according to the Runge–Kutta algorithm described in Section III. In order to avoid very long time simulations and large memory requirements, we have chosen round trip times below 1 μs and a time sampling of 10, i.e., 1 point every 10 is sampled.

Fig. 8 displays the numerical simulations in the time domain showing the splitting of the time scales (a) and the chaos generation (b) as the feedback gain parameter is increased, as observed experimentally. The zoom-in view of the chaotic signal is shown in Fig. 8(c). In the numerical simulations we employ a 300 ns time delay, $\varepsilon = 2 \times 10^{-3}$ to account for the bandpass filtering effect, $\phi_0 = \pi/4$, and $\chi = 1$. We have considered a total simulation time of about 100 μs, that is, about $N = 300$ roundtrips providing a sufficient large number of delay loops to fully observe underlying dynamics induced by the delayed feedback. The modeling results describe the dynamics observed experimentally where the characteristics of the broadband OEO are controlled changing the feedback gain parameter. Although the model can provide a description of the splitting of the time scales

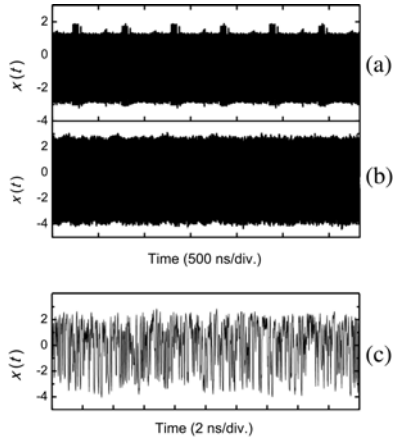

Fig. 8. Numerical simulations of $x(t)$ output with time delay of 300 ns showing the route to chaos dynamics for increasing values of delayed feedback gain: (a) $\beta = 2.0$; (b) $\beta = 3.5$; (c) Zoom-in view of the chaotic signal displayed in (b).

induced by the delay and the chaos generation as observed experimentally, we find that the model does not provide a good description of the fast oscillations measured experimentally. As discussed in [19], this can be attributed to the modeling of the filtering process. As discussed previously, the experimental open loop RF filtering exhibits a maximum at around 2.8 GHz, thus explaining the actual fast oscillations, an effect that is not described by our model.

B. Breather Excitation Dynamics

For applications in the generation of highly stable microwave-photonics signals, increasing the length of the fiber optic delay line results in ultra-low phase noise signals. When operating under high gain conditions time-delayed systems have the potential to produce very high-dimensional dynamics. Recently, it has been found that time-delay systems can display remarkable temporal patterns such as chimera states and chaotic breathers in which the dynamics splits into regular and chaotic components repeating at the time delay interval [30].

In this section we demonstrate that for very large delays and a sufficient high gain conditions the combined influence of the fast and slow times scales yield signals totally different from the ones encountered for instance in Fig. 5(g) and (h), giving rise to hybrid complex signal generation. These behaviors are referred in the literature as breathers and were recently found in other OEO systems employing intensity modulator configurations [18], [19]. The key difference between the breather excitations observed in our OEO is that the slow-scale dynamics reported here repeats at the interval of the delay. Therefore, by increasing the optical fiber delay of the OEO we can achieve different low-scale periodicity without requiring additional changes in the remaining components of the OEO.

In order to investigate such strong asymmetric signal generation, first the OEO is placed in similar gain conditions of Fig. 5(g). The optical delay line is increased to form a total delay of 4.4 μs. Then, by slightly tuning the wavelength of the light to 1558.69 nm, we start to observe the separation of the time scales. As shown in Fig. 3, the effect of tuning the wavelength

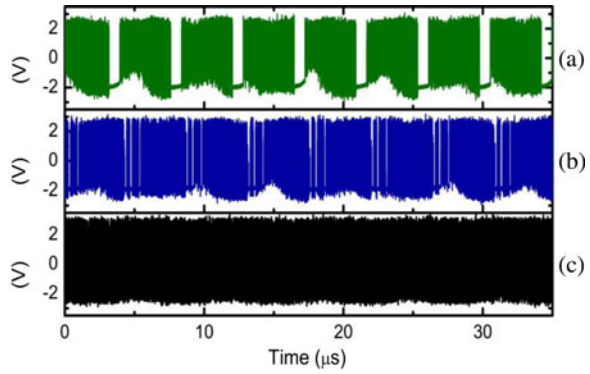

Fig. 9. Experimental large scale time traces of the breather dynamics showing the birth, evolution, and destruction of the breathers as a function of the optical power received by the PD: (a) −3.6 dBm; (b) −3.2 dBm; and (c) −2.2 dBm.

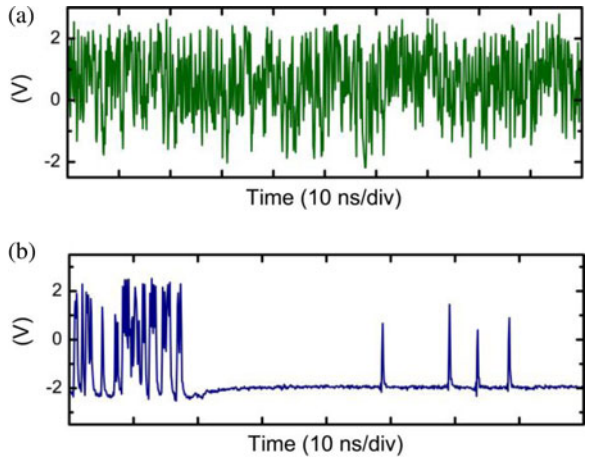

Fig. 10. (a) Enlargement of the experimental time trace (a) of Fig. 9 showing the nanosecond chaotic oscillations within the breathers. (b) Enlargement of time trace (b) of Fig. 9 showing pulsating behavior in the second time interval between nanosecond chaotic oscillations.

produces changes in the MPF bandpass sufficient to enhance and separate the fast and slow multiple time scales of the OEO. Therefore, we observe that before evolving to chaos the OEO can sustain a novel regime of operation—the breathers.

Fig. 9 shows the birth, evolution and destruction of the breather excitations employing a large delay of 4.4 μs as the gain feedback of the OEO is increased. The evolution of the achieved signals shows a drastic change of the time scale behavior of the OEO. While previously we observed oscillations of a period ~0.36 ns [see Fig. 5(c) and (d)], here we observe the formation of an oscillation of a period ~4.4 μs, as shown in Fig. 9(a), which corresponds to a time scale 10^4 times slower. These are hybrid regimes where a fast-scale dynamics is superimposed onto the delay induced slow-scale dynamics. Fig. 10(a) presents an enlargement of the small-scale experimental traces showing a fully developed chaos within the breathers. By tuning the gain conditions we can either enhance or destroy the formation of the breathing phenomena. As shown in Fig. 9(b) and (c), further increase of the gain leads to the destruction of the breathers and the OEO returns to its chaotic regime as shown previously in Fig. 5(i) and (j).

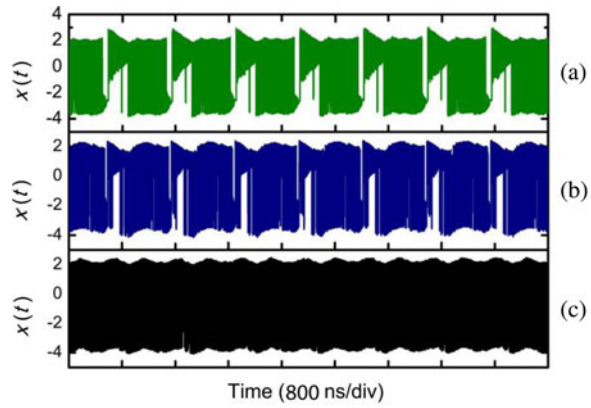

Fig. 11. Numerical simulations of the large scale time traces of the hybrid breather regimes in the $x(t)$ output showing simultaneous slow-scale periodicity and fast-scale nonperiodic signals as a function of the feedback gain parameter: (a) $\beta = 2.82$, (b) $\beta = 2.85$, (c) $\beta = 2.95$.

Interestingly, we also note the fast-slow dynamics presented here also shows signatures of pulsing behavior. The enlargement of the time trace of Fig. 9(b) presented in Fig. 10(b) shows sequences of bursts and single pulsing signals in the transition between the fast and the slow scales. The pulses show identical shape with a sub-nanosecond width. This behavior might be related to multipulse excitability [19], [36] since the achieved pulses have identical shape and amplitude. During the experiments one could not identify a global pattern of the pulse sequences, and the mechanism leading to this kind of self-pulsating is currently being investigated.

The dynamics of the breathers is further confirmed by the numerical simulations, presented in Fig. 11, showing that breather oscillations similar to the signals observed experimentally can be sustained. The numerical simulations presented in Fig. 11 are obtained by employing a time delay of 1 μs. Note that a smaller delay value is used in order to provide a sufficiently large number of delay loops and similar time to step simulation conditions as in the previous sub-section, without requiring much larger computational memory storage. The simulations demonstrate a dependence of the evolution of the breathers with the initial conditions and the strength of the stochastic component. The presence of noise in the system plays a role in the OEO dynamics of either enhancing or destroying the breathing excitations. For the parameters conditions presented in Fig. 11, we find that the use of noise values one order of magnitude above the employed in the simulations can be sufficient to destroy the time scale splitting observed in Fig. 11.

The analysis of these regimes continues further using a space-time representation to analyze any drift or diffusion of the experimental time traces of the breathers. Following a standard procedure, the recorded data is analyzed in a spatially extended representation. This space-time like diagram is a common representation for describing systems with time delay [37], [38]. In this representation, the position of a localized temporal pattern that repeats itself after each round trip is clearly evidenced on a time scale of thousands of cycles. For instance, it was used recently for unveiling an ultra-weak acoustic interaction

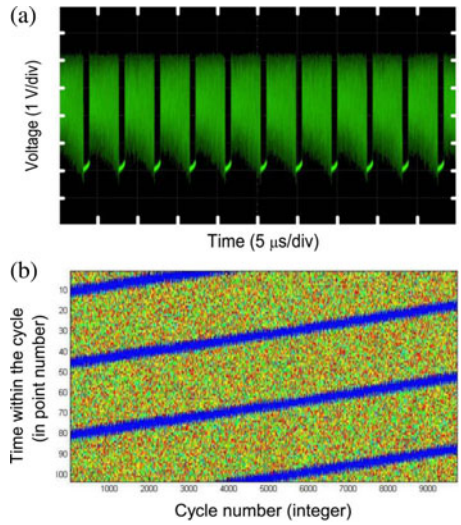

Fig. 12. Analysis of the long term evolution of the breather dynamics. (a) Experimental voltage output of the breather signal when the optical power received by the PD is around −3.6 dBm. (b) Space-time representation for the OEO voltage output with colored amplitude scaling. Time within the cycle (0 to 103) is increasing from top to bottom and corresponds to about three time delay cycles. The horizontal axis, representing the space like direction is in delay units.

between temporal cavity solitons [39]. This writing of the time allows us to reveal the intrinsic multiple time scales of the OEO. In fact, such a representation allows identifying the formation and propagation of "space-time" structures as, e.g., defects and spatiotemporal intermittencies.

We analyze the breathers in the similar conditions shown in Fig. 9(a). A typical signal is displayed in Fig. 12(a) in a time scale of about ten times the delay. In order to map out the breathers in a space-time representation we record the breather displayed in Fig. 12(a) using an acquisition time of about 10^4 the delay and employing a large sampling rate (100 MSa/s). In this space-time representation, shown in Fig. 12(b), we verify the breathers are long and stable waves, where chaotic behaviors are altered, resembling neuronal chaotic bursting [24], [25].

One would like to note that similar signals with a separation of the time scales as the ones shown in Fig. 5(g) have been also observed when the optical carrier is located at the other side of the LCFBG reflection band, although an extensive analysis of the dynamics on the left side of the LCFBG is not performed. However, robust and stable breathing regimes with a strong asymmetry as displayed in Fig. 9 are very difficult to achieve. The different frequency responses, as can be seen from Fig. 3, seem to have an important role in order to achieve the strong time delay scale separation.

Under the experimental conditions reported here, the results show robust and highly-stable generation of breather excitation signals over a time-scale 10^4 times longer than the delay employed. Further investigation on the possibility of drift or diffusion of these regimes is currently underway in order to analyze the possibility for the emergence of novel complex structures such as the excitation of breather solitons recently reported in an optical micro-resonator [28].

V. Conclusion

We have proposed and demonstrated experimentally a broadband OEO that was implemented using a PM and a LCFBG which was used to generate broadband phase-chaotic dynamics. The key contribution of the work was the use of the PM and the LCFBG which jointly operated as a broadband MPF, thus enabling the complex signal generation that includes broadband chaotic signals and breather oscillations resembling neuronal chaotic bursting in which the dynamics splits into regular and chaotic components repeating at the time delay interval. Considering the recent interest in neuronal processing in photonics, such as reservoir computing [40], [41], robust slow-fast scale signals as the ones reported here constitute an interesting example on how different time-scales in an OEO can be employed to achieve novel neuronal-like signal generation in microwave-photonics systems.

The OEO provides attractive and controllable dynamical features, with interest not only in chaos encryption, but also to real time and fast optical processing systems, such as random number generation, photonic ultra-wideband signal generator, and reservoir computing taking advantage of the intrinsic multiple time scales of OEO-based LCFBG systems. In addition, the PM-based OEO eliminates the instability caused by bias drifting in intensity modulator-based architectures and the undesired interference phenomena observed in intensity-modulation chaos encryption OEO systems.

Although the broadband OEO reported here was implemented using discrete devices with large size and high cost, it has the potential to be integrated on a photonic integrated circuit with smaller size and better performance.

References

[1] T. Erneux, *Applied Delayed Differential Equations*. New York, NY, USA: Springer-Verlag, 2009.
[2] M. C. Soriano, J. Garcia-Ojalvo, C. R. Mirasso, and I. Fischer, "Complex photonics: Dynamics and applications of delay-coupled semiconductors lasers," *Rev. Mod. Phys.*, vol. 85, no. 1, pp. 421–470, Mar. 2013.
[3] K. E. Callan, L. Illing, Z. Gao, D. J. Gauthier, and E. Scholl, "Broadband chaos generated by an optoelectronic oscillator," *Phys. Rev. Lett.*, vol. 104, no. 11, p. 113901, Mar. 2010.
[4] A. Argyris, D. Syvridis, L. Larger, V. Annovazzi-Lodi, P. Colet, I. Fischer, J. Garcia-Ojalvo, C. R. Mirasso, L. Pesquera, and K. A. Shore, "Chaos-based communications at high bit rates using commercial fibre-optic links," *Nature*, vol. 438, no. 7066, pp. 343–346, Nov. 2005.
[5] F. Y. Lin and J. M. Liu, "Chaotic lidar," *IEEE J. Sel. Top. Quantum Electron.*, vol. 10, no. 5, pp. 991–997, Sep./Oct. 2004.
[6] Y. C. Wang, B. J. Wang, and A. B. Wang, "Chaotic correlation optical time domain reflectometer utilizing laser diode," *IEEE Photon. Technol. Lett.*, vol. 20, no. 19, pp. 1636–1638, Sep./Oct. 2008.
[7] I. Kanter, Y. Aviad, I. Reidler, E. Cohen, and M. Rosenbluh, "An optical ultrafast random bit generator," *Nature Photon.*, vol. 4, pp. 58–61, Jan. 2010.
[8] J. P. Yao, F. Zeng, and Q. Wang, "Photonic generation of ultra-wideband signals," *J. Lightw. Technol.*, vol. 25, no. 11, pp. 3219–3235, Nov. 2007.
[9] T. B. Simpson, J.-M. Liu, M. AlMulla, N. G. Usechak, and V. Kovanis, "Linewidth sharpening via polarization-rotated feedback in optically injected semiconductor laser oscillators," *IEEE J. Sel. Top. Quantum Electron.*, vol. 19, no. 4, p. 1500807, Jul./Aug. 2013.
[10] J. Zhuang and S. Chan, "Tunable photonic microwave generation using optically injected semiconductor laser dynamics with optical feedback stabilization," *Opt. Lett.*, vol. 38, no. 3, pp. 344–346, Feb. 2013.
[11] T. E. Murphy, A. B. Cohen, B. Ravoori, K. R. B. Schmitt, A. V. Setty, F. Sorrentino, C. R. S. Williams, E. Ott, and R. Roy, "Complex

dynamics and synchronization of delayed-feedback nonlinear oscillators," *Phil. Trans. Roy. Soc. A*, vol. 368, pp. 368–343, Feb. 2010.
[12] G. Kozyreff and T. Erneux, "Singular hopf bifurcation in a differential equation with large state-dependent delay," in *Proc. R. Soc. A*, Feb. 2014, vol. 470, p. 20130596.
[13] J. Ohtsubo, *Semiconductor Lasers: Stability, Instability and Chaos*. London, U.K.: Springer, 2005.
[14] X. Y. Yao and L. Maleki, "Optoelectronic oscillator for photonic systems," *IEEE J. Quantum Electron.*, vol. 32, no. 7, pp. 1141–1149, Jul. 1996.
[15] K. Volyanskiy, P. Salzenstein, H. Tavernier, M. Pogurmirskiy, Y. Chembo, and L. Larger, "Compact optoelectronic microwave oscillators using ultra-high Q whispering gallery mode disk-resonators and phase modulation," *Opt. Exp.*, vol. 18, no. 21, pp. 22358–22363, Oct. 2010.
[16] B. Romeira, J. Javaloyes, J. M. L. Figueiredo, C. N. Ironside, H. I. Cantú, and A. E. Kelly, "Delayed feedback dynamics of liénard-type resonant tunneling-photo-detector optoelectronic oscillators," *IEEE J. Quantum Electron.*, vol. 49, no. 1, pp. 31–42, Jan. 2013.
[17] L. Maleki, D. Eliyahu, and A. B. Matsko, "Optoelectronic oscillator," in *Broadband Optical Modulators: Science, Technology, and Applications*, A. Chen and E. Murphy, Eds. Boca Raton, FL, USA: CRC Press, 2011, pp. 467–488.
[18] Y. C. Kouomou, P. Colet, L. Larger, and N. Gastaud, "Chaotic breathers in delayed electro-optical systems," *Phys. Rev. Lett.*, vol. 95, p. 203903, Nov. 2005.
[19] M. Peil, M. Jacquot, Y. K. Chembo, L. Larger, and T. Erneux, "Routes to chaos and multiple time scale dynamics in broadband bandpass nonlinear delay electro-optic oscillators," *Phys. Rev. E*, vol. 79, p. 026208, Feb. 2009.
[20] L. Weicker, T. Erneux, M. Jacquot, Y. Chembo, and L. Larger, "Crenelated fast oscillatory outputs of a two delay electro-optic oscillator," *Phys. Rev. E*, vol. 85, p. 026206, Feb. 2012.
[21] W. Z. Li and J. P. Yao, "An optically tunable optoelectronic oscillator," *IEEE /OSA J. Lightw. Technol.*, vol. 28, no. 18, pp. 2640–2645, Sep. 2010.
[22] Z. Tang, S. Pan, D. Zhu, R. Guo, Y. Zhao, M. Pan, D. Ben, and J. P. Yao, "Tunable optoelectronic oscillator based on a polarization modulator and a chirped FBG," *IEEE Photon. Technol. Lett.*, vol. 24, no. 17, pp. 1487–1489, Sep. 2012.
[23] K. Ikeda and K. Matsumoto, "High-dimensional chaotic behavior in systems with time-delay feedback," *Physica D*, vol. 29, no. 1–2, pp. 223–235, Nov./Dec. 1987.
[24] T. R. Chay and J. Rinzel, "Bursting, beating, and chaos in an excitable membrane model," *Biophys. J.*, vol. 47, no. 3, pp. 357–366, Mar. 1985.
[25] M. L. Steyn-Ross, D. A. Steyn-Ross, and J. W. Sleigh, "Interacting turing-hopf instabilities drive symmetry-breaking transitions in a mean-field model of the cortex: A mechanism for the slow oscillation," *Phys. Rev. X*, vol. 3, no. 2, p. 021005, May 2013.
[26] A. C. Scott, *Nonlinear Science: Emergence and Dynamics of Coherent Structures*. Lincoln, U.K.: Oxford Univ. Press, 1999.
[27] A. R. McGurn, "Intrinsic localized modes in photonic crystal circuits," *Chaos*, vol. 13, no. 2, pp. 754–765, Jun. 2003.
[28] A. B. Matsko, A. A. Savchenkov, and L. Maleki, "On excitation of breather solitons in an optical microresonator," *Opt. Lett.*, vol. 37, no. 23, pp. 4856–4858, Dec. 2012.
[29] F. Zeng and J. P. Yao, "Ultrawideband impulse radio signal generation using a high-speed electrooptic phase modulator and a fiber-Bragg-grating-based frequency discriminator," *IEEE Photon. Technol. Lett.*, vol. 18, no. 19, pp. 2062–2064, Sep./Oct. 2006.
[30] L. Larger, B. Penkovsky, and Y. Maistrenko, "Virtual chimera states for delayed-feedback systems," *Phys. Rev. Lett.*, vol. 111, p. 054103, Aug. 2013.
[31] R. Lavrov, M. Peil, M. Jacquot, L. Larger, V. Udaltsov, and J. Dudley, "Electro-optic delay oscillator with nonlocal nonlinearity: Optical phase dynamics, chaos, and synchronization," *Phys. Rev. E*, vol. 80, p. 026207, Aug. 2009.
[32] C. W. Gardiner, *Handbook of Stochastic Methods. H. Haken*. Berlin, Germany: Springer-Verlag, 1985.
[33] W. H. Press, S. A. Teukolsky, W. T. Vetterling, and B. P. Flannery, *The Art of Scientific Computing*. Cambridge, U.K.: Cambridge Univ. Press, 2007.
[34] J. W. Eaton, *GNU Octave Manual*. Surrey, U.K.: Network Theory Publishing, 2002.
[35] A.2 Mex-Files. (2010). [Online]. Available: http://www.gnu.org/software/octave/doc/interpreter/Mex_002dFiles.html
[36] B. Romeira, J. Javaloyes, C. N. Ironside, J. M. L. Figueiredo, S. Balle, and O. Piro, "Excitability and optical pulse generation in semiconductor lasers driven by resonant tunneling diode photo-detectors," *Opt. Exp.*, vol. 21, no. 18, pp. 20931–20940, 2013.
[37] G. Giacomelli, R. Meucci, A. Politi, and F. T. Arecchi, "Defects and space-like properties of delayed dynamical systems," *Phys. Rev. Lett.*, vol. 73, no. 8, pp. 1099–1102, Aug. 1994.
[38] G. Giacomelli and A. Politi, "Relationship between delayed and spatially extended dynamical systems," *Phys. Rev. Lett.*, vol. 76, pp. 2686–2689, Apr. 1996.
[39] J. K. Jang, M. Erkintalo, S. G. Murdoch, and S. Coen, "Ultraweak long-range interactions of solitons observed over astronomical distances," *Nature Photon.*, vol. 7, no. 8, pp. 657–663, Aug. 2013.
[40] J. Campenhout, "Toward optical signal processing using photonic reservoir computing," *Opt. Exp.*, vol. 16, no. 15, pp. 182–192, 2008.
[41] Y. Paquot, F. Duport, A. Smerieri, J. Dambre, B. Schrauwen, M. Haelterman, and S. Massar, "Optoelectronic reservoir computing," *Sci. Rep.*, vol. 2, no. 287, pp. 1–6, Feb. 2012.

Bruno Romeira (M'13) received the five-year diploma degree in physics and chemistry from the University of the Algarve, Faro, Portugal, in 2006, and the Ph.D. degree in physics (*summa cum laude*) and the title of European Ph.D. at the same university, jointly with the University of Glasgow, Glasgow, U.K., and the University of Seville, Seville, Spain, in 2012.

He is currently engaged in a Postdoctoral Fellowship program at the Center of Electronics Optoelectronics and Telecommunications (CEOT), Department of Physics, University of the Algarve, and at the Microwave Photonics Research Laboratory, University of Ottawa, Ottawa, ON, Canada, as a visiting Postdoc. His research cuts across several disciplines in applied physics and engineering, which include semiconductor physics, solid-state electronics and optoelectronics. His research interests include complex systems, chaos, and synchronization for novel applications in information and communication technologies.

Dr. Romeira received, in 2009, the "Young Researchers Incentive Programme" award from the Calouste Gulbenkian Foundation, Portugal, and he is one of the recipients of the "IEEE Photonics Society Graduate Student Fellowship" (2011), from the IEEE Photonics Society, USA. His Ph.D. thesis entitled "Dynamics of Resonant Tunneling Diode Optoelectronic Oscillators" was awarded the "Best Ph.D. Thesis in Optics and Photonics in Portugal in 2012" by the Portuguese Society of Optics and Photonics (SPOF).

Fanqi Kong (S'13) received the B.Eng. degree in optoelectronics information engineering from Huazhong University of Science and Technology, Wuhan, China, in 2012. He is currently working toward the M.A.Sc. degree in the School of Electrical Engineering and Computer Science, University of Ottawa, Ottawa, ON, Canada.

His current research interests include photonic generation of microwave signals and applications in sensing systems.

Wangzhe Li (S'08) received the B.E. degree in electronic science and technology from Xi'an Jiaotong University, Xi'an, China, in 2004, the M.Sc. degree in optoelectronics and electronic science from Tsinghua University, Beijing, China, in 2007, and the Ph.D. degree in electrical engineering from the University of Ottawa, Ottawa, ON, Canada, in 2013.

He is currently a Postdoctoral Researcher working at the Microwave Photonics Research Laboratory, School of Electrical Engineering and Computer Science, University of Ottawa, Ottawa, ON, Canada. His current research interests include photonic generation of microwave and terahertz signals, arbitrary waveform generation, optoelectronic oscillation, and silicon photonics.

Dr. Li was a recipient of the 2011 IEEE Microwave Theory and Techniques Society Graduate Fellowship and the 2011 IEEE Photonics Society Graduate Fellowship.

José M. L. Figueiredo (M'09) received the B.Sc. degree in physics (optics and electronics) in 1991 and the M.Sc. degree in optoelectronics and lasers in 1997, both from the University of Porto, Porto, Portugal. In 2000, he received the Ph.D. degree in physics from the same university in "co-tutela" with the University of Glasgow, Glasgow, U.K., where he worked on the optoelectronic properties of resonant tunneling diodes.

In 1999 he joined to the Department of Physics, University of the Algarve, Faro, Portugal. His current research interests include resonant tunneling diode microwave and millimeter-wave oscillators, the generation of microwave-photonic signals, generation of chaotic signals; terahertz communications.

Julien Javaloyes (M'11) was born in Antibes, France. He received the M.Sc. degree in physics from the École Normale Supérieure de Lyon, Lyon, France, and the Ph.D. degree in physics from the Institut Non Linéaire de Nice, Université de Nice Sophia Antipolis, Nice, France, where he studied the recoil induced instabilities and self-organization processes occurring in cold atoms.

He worked on delay induced dynamics in coupled semiconductor lasers during a postdoctoral stage in Brussels, Belgium, and on VCSEL polarization dynamics in Palma de Mallorca, Spain. He was a Research Associate with Glasgow University, Glasgow, U.K., where provided for the modeling of the dynamics of monolithic semiconductor diodes. He joined the Department of Physics, Universitat de les Illes Balears, Palma, Spain, in 2010, as a Ramón y Cajal Fellow. His current research interests include laser dynamics, atom-light interaction modeling and applied numerical bifurcation analysis.

Jianping Yao (M'99–SM'01–F'12) received the Ph.D. degree in electrical engineering from the Université de Toulon, Toulon, France, in December 1997.

He joined the School of Electrical Engineering and Computer Science, University of Ottawa, Ottawa, ON, Canada, as an Assistant Professor in 2001, where he became an Associate Professor in 2003 and a Full Professor in 2006. He was appointed the University Research Chair in Microwave Photonics in 2007. From July 2007 to June 2010, he was the Director of the Ottawa-Carleton Institute for Electrical and Computer Engineering. Prior to joining the University of Ottawa, he was an Assistant Professor in the School of Electrical and Electronic Engineering, Nanyang Technological University, Singapore, from 1999 to 2001. He has published more than 430 papers, including more than 250 papers in peer-reviewed journals, and 180 papers in conference proceedings. He is a Chair of numerous international conferences, symposia, and workshops, including the Vice-TPC Chair of the 2007 IEEE Microwave Photonics Conference, TPC Co-chair of the 2009 and 2010 Asia-Pacific Microwave Photonics Conferences, TPC Chair of the high-speed and broadband wireless technologies subcommittee of the 2009–2012 IEEE Radio Wireless Symposia, TPC Chair of the microwave photonics subcommittee of the 2009 IEEE Photonics Society Annual Meeting, TPC Chair of the 2010 IEEE Microwave Photonics Conference, and General Co-Chair of the 2011 IEEE Microwave Photonics Conference. He also serves as an IEEE distinguished microwave Lecturer for 2013–2015. He is a registered Professional Engineer of Ontario. He is a Fellow of the Optical Society of America, and a Fellow of the Canadian Academy of Engineering.

Dr. Yao received the 2005 International Creative Research Award at the University of Ottawa. He was the recipient of the 2007 George S. Glinski Award for Excellence in Research. He was selected to receive an inaugural OSA outstanding reviewer award in 2012.